High-Spatial-Resolution Strain Sensor Based on Rayleigh-Scattering-Enhanced SMF Using Direct UV Exposure

Chao Du, Cailing Fu, Pengfei Li, Yanjie Meng, Huajian Zhong, Bin Du, Kuikui Guo, Lin Chen, Yiping Wang, *Senior Member, IEEE*, and Jun He, *Member, IEEE*

***Abstract*—A high-spatial-resolution, i.e., 2.0 mm, strain sensor based on a Rayleigh-scattering-enhanced SMF, i.e., exposed SMF (E-SMF) with direct UV laser, was experimentally demonstrated. The enhancement of Rayleigh-scattering (RS) intensity could be tuned by adjusting the exposure parameters, i.e., distance between SMF and Phase mask, energy of UV laser and velocity of the SMF. A 1.0 m long E-SMF with a RS enhancement of 37.3 dB was obtained, where the exposure time was only 100 s. Compared with the unexposed SMF (UE-SMF), the strain profiles of the E-SMF could be clearly demodulated without fluctuation at a spatial resolution of 2.0 mm using traditional cross-correlation algorithm when the applied strain was from 200 to 2600 $\mu\varepsilon$.**

***Index Terms*—Distributed strain sensor, optical frequency domain reflectometer, Rayleigh scattering, UV exposure.**

I. Introduction

DISTRIBUTED optical fiber strain sensor based on Rayleigh scattering (RS) has attracted great attention owing to its potential applications in various fields, such as industrial infrastructure monitoring [1], [2], [3] and shape sensing [4], [5]. Among them, distributed strain sensing technology based on RS could be divided into two categories, i.e., optical time domain reflectometry (OTDR) [6] and optical frequency domain reflectometry (OFDR) [7]. Compared with OTDR, the OFDR exhibited a high spatial resolution, i.e., centimeters or even millimeters scale [8], [9]. However, a higher spatial resolution and accuracy was limited by the inherent weak RS signal in the conventional optical fiber, i.e., single mode fiber (SMF). Recently, various methods have been proposed and demonstrated to enhance the RS intensity in fiber. Specialty designed fibers, such as polymer fiber with a larger cross-section [10] and silica fiber doped with various nanoparticles, i.e., MgO [11], [12] and Ca [13], in the core were fabricated to enhance the RS intensity. Moreover, weak fiber gratings [14], weak reflectors [15], random fiber gratings [16], and nano fiber gratings [17], and fabricated by femtosecond laser were also used to enhance the RS intensity. Among them, nanoparticles doped preforms should be prepared to obtain the specialty designed fibers, which increased the complexity of the experiment [11], [12], [13]. Besides, the spatial resolution of the weak fiber gratings and reflectors was dependent on the interval in the fabrication process [14], [15]. Loranger et al. proposed and demonstrated a simple and affordable method, i.e., exposing the fiber core to UV light, to generate a 20 dB increase in RS signal for SMF and high Ge-doped core fiber [18]. However, the RS intensity could only be enhanced when the SMF was located at the focus position, where the position of fiber should be accurately adjusted [18].

In this letter, we experimentally demonstrated a high-spatial-resolution strain sensor based on a RS-enhanced SMF, i.e., an exposed-SMF (E-SMF) exposed with direct UV laser at defocus position. The dependence of RS intensity enhancement on the exposure parameters, such as distance between SMF and phase mask, energy of UV laser and velocity of the SMF, were investigated to obtain a higher enhancement of the RS intensity. Moreover, the root mean square (RMS) noise level of the E-SMF at different gage lengths, i.e., spatial resolutions, was also studied. Furthermore, the strain properties of the E-SMF and un-exposed SMF (UE-SMF) were also investigated and compared.

II. Experimental Setup and Methods

A. Experimental Setup

An experimental setup based on direct UV exposure was built to enhance the RS of the SMF, as illustrated in Fig. 1(a). Note that

Manuscript received 14 May 2022; revised 12 October 2022 and 3 November 2022; accepted 16 November 2022. Date of publication 23 November 2022; date of current version 3 March 2023. This work was supported in part by the National Natural Science Foundation of China under Grants 61905155 and U1913212, in part by the Natural Science Foundation of Guangdong Province under Grants 2019B1515120042, 2019A1515011393, 2021A1515110167 and 2021A1515011925, in part by the Science and Technology Innovation Commission of Shenzhen under Grants JCYJ20200109114020865, JCYJ20200109114201731, 20200810121618001, and JCYJ20210324100008024, and in part by the Shenzhen Key Laboratory of Photonic Devices and Sensing Systems for Internet of Things. *(Corresponding author: Cailing Fu.)*

Chao Du, Cailing Fu, Pengfei Li, Yanjie Meng, Huajian Zhong, Bin Du, Kuikui Guo, Lin Chen, Yiping Wang, and Jun He are with the Key Laboratory of Optoelectronic Devices and Systems of Ministry of Education and Guangdong Province, College of Physics and Optoelectronic Engineering, Shenzhen University, Shenzhen 518060, China, and also with the Shenzhen Key Laboratory of Photonic Devices and Sensing Systems for Internet of Things, Guangdong and Hong Kong Joint Research Centre for Optical Fiber Sensors, Shenzhen University, Shenzhen 518060, China (e-mail: duchao2020@email.szu.edu.cn; fucailing@szu.edu.cn; lipengfei2022@163.com; mengyanjie2020@email.szu.edu.cn; 2060453029@email.szu.edu.cn; dubean@126.com; 2150190116@email.szu.edu.cn; 2070456043@email.szu.edu.cn; ypwang@szu.edu.cn; hejun07@szu.edu.cn).

Color versions of one or more figures in this article are available at https://doi.org/10.1109/JLT.2022.3224311.

Digital Object Identifier 10.1109/JLT.2022.3224311

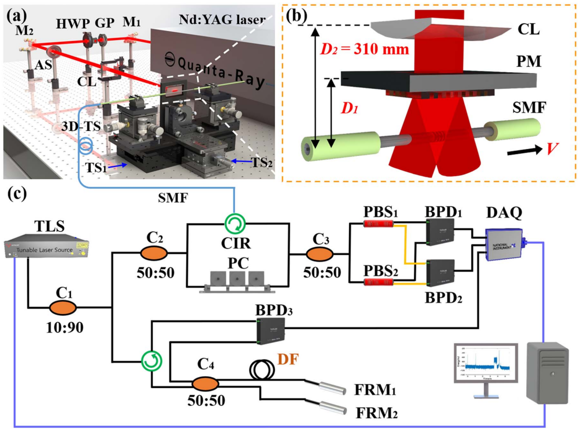

Fig. 1. (a) Experimental setup based on direct UV exposure to enhance the Rayleigh scattering (RS) of single mode fiber (SMF); (b) Enlarged schematic diagram of the exposure area, where D_1 and D_2 are the distance of the SMF from PM and CL, respectively; (c) Schematic diagram of optical frequency domain reflectometry (OFDR) to measure the RS signal of the SMF. M: mirror; GP: Glan-prism polarizer; HWP: half-wave plate; AS: aperture stop; CL: cylindrical lens, PM: phase mask; TS: translation stage; TLS: tunable laser source; C: coupler; CIR: circulator; DF: delay fiber; FRM: faraday rotating mirror; BPD: balanced photo-detector; PC: polarization controller; PBS: polarization beam splitter; DAQ: data acquisition card.

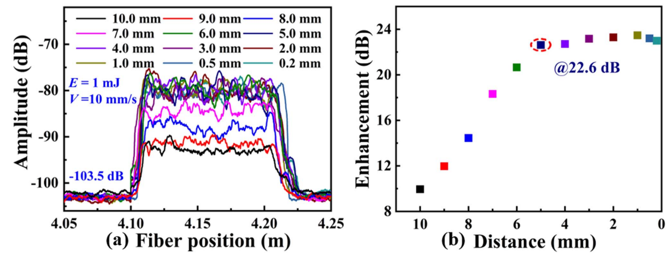

Fig. 2. (a) Obtained RS intensity signal of the RS-enhanced SMF, i.e., E-SMF, based on OFDR when the distance between SMF and PM, i.e., D_1, was decreased from 10.0 to 0.2 mm; (b) The measured average RS intensity enhancement of the E-SMF as a function of the distance between SMF and PM, i.e., D_1. Note that the energy of UV laser and the velocity of the TS_1, i.e., the moving velocity of the SMF, were set to 1 mJ and 10.0 mm/s; 0 dB was defined as the RS intensity enhancement of un-exposed SMF (UE-SMF).

the SMF was hydrogen loaded at 80 °C and 13 MPa for 7 days to enhance the photosensitivity before direct UV exposure. A pulse laser (Quantum-Ray Lab-170, Spectra Physics, 1064 nm) with a fourth harmonic generator was used to produce an UV laser with a wavelength and repetition rate of 266 nm and 10 Hz, respectively. The generated UV laser was employed to directly expose the SMF after passing through mirror_1 (M_1), half-wave plate (HWP), Glan-prism polarizer (GP), mirror_2 (M_2), aperture stop (AS), long-focus cylindrical lens (CL) and phase mask (PM), where the focal length of the CL and the period of PM were 300 mm and 1065 nm, respectively. The variable attenuator composed of HWP and GP was used to adjust the laser energy between 0.1 and 100 mJ. Two ends of the SMF were fixed by the dual-arm fiber holders installed on the three-dimensional translation stage (3D-TS), which was used to adjust the SMF to be parallel to the PM. To realize the exposure on SMF with a certain length rather than a single point, a one-dimensional (1D) electric translation stage1 i.e., TS_1, was employed to drive the SMF to move continuously along the fiber axis at a velocity of V during the UV exposure. In addition, the PM was fixed on another 1D translation stage2, i.e., TS_2, which was used to adjust the distance between the SMF and PM, i.e., D_1, as illustrated in Fig. 1(b). Note that the distance between CL and SMF was remained at 310 mm, i.e., $D_2 = 310$ mm, indicating that the SMF was located at the defocus position in the experiment as the focal length of the CL was 300 mm. Compared with Ref. [18], the complexity of accurately adjusting the fiber at the focus position was reduced, which was conducive to the exposure of long-distance SMF.

As shown in Fig. 1(c), an experimental setup based on optical frequency domain reflectometry (OFDR) was built to measure the RS signal of the SMF. Light from a tunable laser source (TLS) was divided into two parts, i.e., main interferometer (MI) and auxiliary interferometer (AI), by a 10:90 coupler (C_1). The MI was consisted of C_2, circulator (CIR), polarization controller (PC), and C_3, while the AI was consisted of two faraday rotating mirrors, i.e., FRM_1 and FRM_2, delay fiber (DF), and C_4. Two polarization beam splitters, i.e., P were used to split the signal into p- and s-polarization light, and the balanced photo-detector (BPD) was used to convert the obtained signal into electrical signal and then collected by DAQ for the data processing. Note that the sweep range and sweep rate of the TLS were 10 nm and 80 nm/s, respectively.

B. Scattering Enhanced Fiber Fabrication

The detailed process to obtain a RS-enhanced SMF, i.e., exposed SMF (E-SMF) with an enhanced RS, was as follows. Firstly, a section of hydrogen-loaded SMF was fixed by two dual-arm fiber holders after removing the coating, where the distance between SMF and PM, i.e., D_1, should be adjusted. Then the hydrogen-loaded SMF was exposed with an appropriate energy of UV laser, i.e., E, while the SMF was continuously moved at a velocity of V. At the same time, the RS signal of the exposed SMF (E-SMF) was measured in real time based on OFDR in Fig. 1(c). Obviously, the enhanced RS intensity was dependent on the exposure parameters during the direct UV exposure, such as the distance between SMF and PM, i.e., D_1, the energy of UV laser, i.e., E, and the moving velocity of the SMF, i.e., V, which were analyzed in detail as follows.

Firstly, the effect of the distance between SMF and PM, i.e., D_1, on the RS intensity enhancement was investigated. Note that the energy of UV laser and the velocity of the TS_1, i.e., the moving velocity of the SMF, were set to 1 mJ and 10.0 mm/s in the experiment. As shown in Fig. 2(a), the exposure area was ranged from 4.10 to 4.22 m, i.e., an E-SMF with a length of 12 cm was obtained. Compared with the RS intensity of -103.5 dB for the un-exposed SMF (UE-SMF), i.e., fiber from 4.05 to 4.10 m, the average RS intensity was increased to -93.5 dB when the distance between SMF and PM was 10.0 mm, i.e., $D_1 = 10.0$ mm, labeled by the black curve in Fig. 2(a). This indicated that an average RS intensity enhancement of 10 dB in 12 cm length was obtained by exposing the SMF with direct UV laser, as illustrated by the black dot in Fig. 2(b). Note that the 0 dB

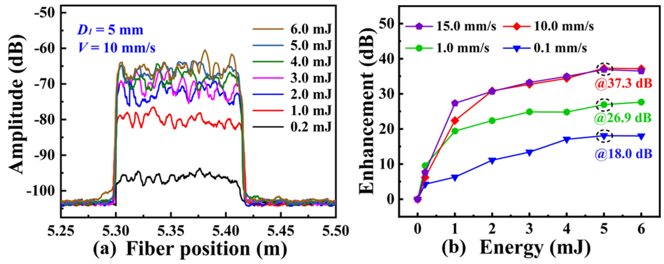

Fig. 3. (a) Obtained RS intensity signal of the E-SMF when the applied laser energy was increased from 0.2 to 6.0 mJ; Note that the distance, i.e., D_1, and velocity of the SMF, i.e., V, were set to 5 mm and 10.0 mm/s; (b) The measured average RS intensity enhancement of the E-SMF as a function of the applied laser energy, when the velocity of the SMF, i.e., V, was 15.0(purple),10.0 (blue), 1.0 (green), and 0.1 mm/s (red), respectively.

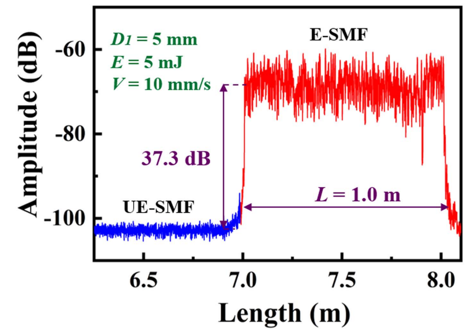

Fig. 4 Obtained RS intensity signal of the E-SMF with a length of 1.0 m, i.e., $L = 1.0$ m, when the optimal exposure parameters, i.e., distance between SMF and phase mask, energy of UV laser and velocity of the SMF, were set to 5 mm, 5 mJ, and 10 mm/s.

was defined as the RS intensity enhancement of UE-SMF. In addition, the RS signal of hydrogen loaded SMF is the same as that of UE-SMF. It is obvious that the average RS intensity enhancement of the E-SMF was increased from 10 to 22.6 dB with the decrease of the distance, i.e., D_1, from 10.0 to 5.0 mm. Then the average RS intensity enhancement was remained at approximately 22.6 dB with the further decrease of D_1, i.e., from 4 to 0.2 mm, indicating that a saturation point of average RS intensity enhancement was achieved. Therefore, the optimal distance between SMF and PM was 5 mm, i.e., $D_1 = 5$ mm, where the average RS intensity enhancement was up to 22.6 dB.

Secondly, the effect of the UV laser energy, i.e., E, on the RS intensity enhancement was also investigated. Note that the distance between SMF and PM was set to 5 mm, i.e., $D_2 =$ 5 mm, corresponding to the optimal distance in Fig. 2. As shown in Fig. 3(a), the average RS intensity of the E-SMF with a length of 12 cm was increased from -103.5 to -66.2 dB, i.e., an average RS intensity enhancement of 37.3 dB, when the SMF was continuously moved with a velocity of 10 mm/s, i.e., $V =$ 10 mm/s, during UV exposure process. Obviously, the average RS intensity of the E-SMF was increased rapidly and then slowly until saturation, when the applied UV laser energy was increased from 0.2 to 6.0 mJ at a constant moving velocity of 10 mm/s, as illustrated by red curve in Fig. 3(b).

Finally, the effect of the velocity of the SMF, i.e., V, on the RS intensity enhancement was investigated. As shown in Fig. 3(b), three other velocities of 15.0, 1.0 and 0.1 mm/s, i.e., $V = 15.0$, 1.0, 0.1 mm/s, were also applied. The average RS intensity at the same velocity exhibited a similar trend, i.e., it was increased rapidly and then slowly until saturation with the increase of the applied laser energy. And the energy of UV laser corresponding to the saturation point at four velocities was kept at 5 mJ, i.e., $E =$ 5 mJ. Moreover, the maximum RS intensity enhancement of the velocity of 15.0 and 10.0 mm/s, i.e., 37.3 dB, was greater than that of the velocity of 1.0 and 0.1 mm/s, i.e., 26.9 and 18.0 dB. Note that the maximum RS intensity enhancement of 15.0 mm/s was equivalent to that of 10.0 mm/s. Therefore, the velocity of 10.0 mm/s was finally selected based on the repeatability and production efficiency.

According to the experimental results in Figs. 2 and 3, we could conclude that the optimal exposure parameters were $D_1 = 5$ mm, $E = 5$ mJ, $V = 10$ mm/s. As shown in Fig. 4, the E-SMF with a length of 1.0 m, i.e., $L = 1.0$ m, was obtained with afore-mentioned optimal exposure parameters, where the enhancement of RS intensity could be up to 37.3 dB. Moreover, the loss of the obtained E-SMF was approximately 0.06 dB/m by comparing the RS intensity of the UE-SMF and E-SMF, corresponding to -104.32 dB and -104.38 dB, respectively. Compared to the velocity of 0.1 mm/s in Ref. [17], only 100 s was spent for exposing a 1.0 m long SMF at an optimal velocity of 10.0 mm/s, which greatly improved the exposure efficiency. In addition, the enhancement of RS intensity could be adjusted by combining exposure parameters.

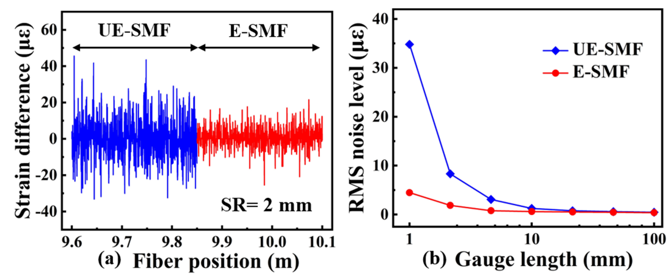

Fig. 5 (a) Noise level, i.e., strain difference, of un-exposed SMF (UE-SMF) and E-SMF, i.e., RS-enhanced SMF, without strain under the spatial resolution of 2.0 mm, labeled by blue and red curve, respectively; (b) Root mean square (RMS) noise level comparison between UE-SMF and E-SMF, when the gauge length, i.e., spatial resolution, was varied from 1 to 100 mm.

III. Research on Strain Sensing Characteristics

In order to investigate the strain sensing properties of the RS-enhanced SMF, the noise levels, i.e., strain differences, of UE-SMF and E-SMF without strain were firstly compared and analyzed. Note the noise level, i.e., strain difference, was defined as the strain fluctuation of UE-SMF and E-SMF under zero strain, i.e., the measurement error. The RS-enhanced SMF, i.e., E-SMF, fabricated under the optimal parameters was used as a sample to measure the noise level, where the RS intensity enhancement was 37.3 dB. As show in Fig. 5(a), the strain differences of the UE-SMF and E-SMF were compared under a spatial resolution of 2.0 mm, which are labeled by blue and red curve, respectively. It is obvious that the strain difference of the

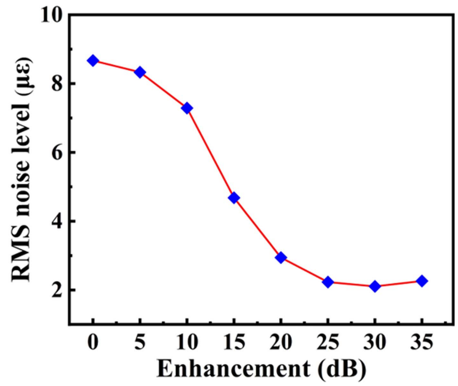

Fig. 6 RMS noise level as a function of the RS intensity enhancement, when the spatial resolution was 2 mm.

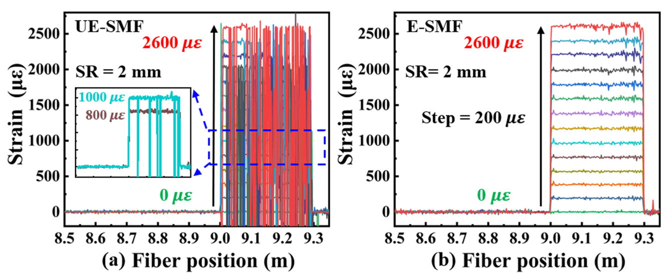

Fig. 7 Demodulated strain profiles of (a) UE-SMF and (b) E-SMF using traditional cross-correlation algorithm while the strain was increased from 200 to 2600 $\mu\varepsilon$ with a step of 200 $\mu\varepsilon$, where the spatial resolution was 2.0 mm. Inset: enlarged view of demodulated strain profiles at 800 and 1000 $\mu\varepsilon$.

E-SMF, i.e., 20 $\mu\varepsilon$, was much lower than that of UE-SMF, i.e., 50 $\mu\varepsilon$. Moreover, the root mean square (RMS) noise levels of the UE-SMF and E-SMF at different gage lengths, i.e., spatial resolutions, were also studied. As shown in Fig. 5(b), the RMS noise level change of the UE-SMF and E-SMF were 35 and 5 $\mu\varepsilon$, respectively, when the gage length was varied from 1 to 100 mm. Moreover, the RMS noise level of the E-SMF was much lower than that of the UE-SMF, when the spatial resolution was between 1 and 10 mm, i.e., 1$\sim$10 mm, attributing to a stronger RS signal of the E-SMF, i.e., a higher signal-to-noise ratio, than UE-SMF. This indicated that the RMS noise level was greatly reduced by using RS-enhanced SMF, i.e., E-SMF.

Furthermore, the RMS noise levels under different RS intensity enhancements were evaluated at the spatial resolution of 2 mm. The seven E-SMF samples with an average RS intensity enhancement of 5, 10, 15, 20, 25, 30, and 35 dB were obtained by adjusting the exposure parameters. As shown in Fig. 6, the stronger the RS intensity enhancement, the lower the RMS noise level. When the RS intensity enhancement was stronger than 25 dB, the RMS noise level, i.e., 2 $\mu\varepsilon$, could not be further reduced due to the environmental fluctuations. Therefore, the E-SMF with a RS intensity enhancement of 25 dB was selected for the following strain test.

As shown in Fig. 7, the strain properties of the UE-SMF and E-SMF were measured and compared using traditional cross-correlation algorithm based on OFDR [19]. One end of the sample fiber was fixed, other end was fixed on a 1D translation stage used to apply the strain along the fiber axis, where the length of the sample fiber, i.e., UE-SMF and E-SMF, was 30 cm, i.e., from 9.0 m to 9.3 m. The demodulated strain profiles of UE-SMF and E-SMF using traditional cross-correlation algorithm were illustrated in Fig. 7(a) and (b), when the strain was increased from 200 to 2600 $\mu\varepsilon$ with a step of 200 $\mu\varepsilon$ and the spatial resolution was 2.0 mm. As shown in Fig. 7(a), the strain profile for the UE-SMF could be clearly demodulated when the applied strain was less than 800 $\mu\varepsilon$. However, the signal for the UE-SMF was submerged in noise when the applied strain was greater than 800 $\mu\varepsilon$, i.e., 1000$\sim$2600 $\mu\varepsilon$. In contrast, the demodulated strain profile of E-SMF with a RS enhancement intensity of 25 dB could be clearly identified without fluctuation when the applied strain was between 0 and 2600 $\mu\varepsilon$, as illustrated in Fig. 7(b). This indicated that the sensing performance could be greatly improved by using an RS-enhanced SMF, i.e., E-SMF.

IV. Conclusion

In conclusion, a high-spatial-resolution, i.e., 2.0 mm, strain sensor was demonstrated based on a RS-enhanced SMF, i.e., E-SMF by direct UV laser. The SMF was located at the defocus position to enhance the RS intensity, which greatly improved the exposure efficiency and reduced the complexity of accurately adjusting the fiber. The optimal exposure parameters of distance between SMF and PM, energy of UV laser, and velocity of the SMF were $D_1 = 5$ mm, $E = 5$ mJ, $V = 10$ mm/s, respectively. A 1.0 m long E-SMF with a RS enhancement of 37.3 dB was obtained, where the exposure time was only 100 s. The strain profiles of the E-SMF could be clearly demodulated at a spatial resolution of 2.0 mm using traditional cross-correlation algorithm when the applied strain was from 200 to 2600 $\mu\varepsilon$. Hence, the sensing performance could be greatly improved by using an RS-enhanced SMF.

References

[1] C. M. Monsberger and W. Lienhart, "Distributed fiber optic shape sensing of concrete structures," *Sensors*, vol. 21, no. 18, Sep. 2021, Art. no. 6098.

[2] S. Rizzolo et al., "Real time monitoring of water level and temperature in storage fuel pools through optical fibre sensors," *Sci. Rep.*, vol. 7, no. 1, Aug. 2017, Art. no. 8766.

[3] L. Peng, J. W. Li, R. A. McLaughlin, H. Ebendorff-Heidepriem, and S. C. Warren-Smith, "Distributed optical fiber sensing of micron-scale particles," *Sens. Actuator A-Phys.*, vol. 303, Mar. 2020, Art. no. 111762.

[4] G. K. Sun, H. Li, M. L. Dong, X. P. Lou, and L. Q. Zhu, "Optical fiber shape sensing of polyimide skin for a flexible morphing wing," *Appl. Opt.*, vol. 56, no. 33, pp. 9325–9332, Nov. 2017.

[5] Y. J. Meng et al., "Shape sensing using two outer cores of multicore fiber and optical frequency domain reflectometer," *J. Lightw. Technol.*, vol. 39, no. 20, pp. 6624–6630, Oct. 2021.

[6] P. Lu et al., "Distributed optical fiber sensing: Review and perspective," *Appl. Phys.*, vol. 6, no. 4, Dec. 2019, Art. no. 041302.

[7] Z. Y. Ding et al., "Distributed optical fiber sensors based on optical frequency domain reflectometry: A review," *Sensors*, vol. 18, no. 4, Apr. 2018, Art. no. 1072.

[8] S. Qu et al., "High spatial resolution investigation of OFDR based on image denoising methods," *IEEE Sensors J.*, vol. 21, no. 17, pp. 18871–18876, Sep. 2021.

[9] P. F. Li et al., "High-spatial-resolution strain sensor based on distance compensation and image wavelet denoising method in OFDR," *J. Lightw. Technol.*, vol. 39, no. 19, pp. 6334–6339, Oct. 2021.

[10] S. T. Kreger, A. K. Sang, D. K. Gifford, and M. E. Froggatt, "Distributed strain and temperature sensing in plastic optical fiber using Rayleigh scatter," *Proc. SPIE*, vol. 7316, 2009, Art. no. 73160.

[11] M. Sypabekova et al., "Fiber optic refractive index sensors through spectral detection of Rayleigh backscattering in a chemically etched MgO-based nanoparticle-doped fiber," *Opt. Lett.*, vol. 43, no. 24, pp. 5945–5948, Dec. 2018.

[12] A. Beisenova et al., "Simultaneous distributed sensing on multiple MgO-doped high scattering fibers by means of scattering-level multiplexing," *J. Lightw. Technol.*, vol. 37, no. 13, pp. 3413–3421, Jul. 2019.

[13] V. Fuertes et al., "Engineering nanoparticle features to tune Rayleigh scattering in nanoparticles-doped optical fibers," *Sci. Rep.*, vol. 11, no. 1, Apr. 2021, Art. no. 9116.

[14] B. J. Xu et al., "Femtosecond laser point-by-point inscription of an ultra-weak fiber Bragg grating array for distributed high-temperature sensing," *Opt. Exp.*, vol. 29, no. 20, pp. 32615–32626, Sep. 2021.

[15] Z. Q. Peng et al., "Identifications and classifications of human locomotion using Rayleigh-enhanced distributed fiber acoustic sensors with deep neural networks," *Sci. Rep.*, vol. 10, no. 1, Dec. 2020, Art. no. 21014.

[16] P. Lu, S. J. Mihailov, D. Coulas, H. M. Ding, and X. Y. Bao, "Low-Loss random fiber gratings made with an fs-IR laser for distributed fiber sensing," *J. Lightw. Technol.*, vol. 37, no. 18, pp. 4697–4702, Sep. 2019.

[17] A. D. Yan et al., "Distributed optical fiber sensors with ultrafast laser enhanced Rayleigh backscattering profiles for real-time monitoring of solid oxide fuel cell operations," *Sci. Rep.*, vol. 7, no. 1, Aug. 2017, Art. no. 9360.

[18] S. Loranger, M. Gagne, V. Lambin-Iezzi, and R. Kashyap, "Rayleigh scatter based order of magnitude increase in distributed temperature and strain sensing by simple UV exposure of optical fibre," *Sci. Rep.*, vol. 5, no. 11777, pp. 1–7, Jun. 2015.

[19] Y. Du et al., "Cryogenic temperature measurement using Rayleigh backscattering spectra shift by OFDR," *IEEE Photon. Technol. Lett.*, vol. 26, no. 11, pp. 1150–1153, Jun. 2014.

Chao Du was born in Shanxi, China, in 1998. He received the B.S. degree from the School of Physics and Optoelectronic Engineering, Taiyuan University of Technology, Taiyuan, China, in 2020. He is currently working toward the M.S. degree in optical engineering with Shenzhen University, Shenzhen, China.

Cailing Fu was born in Hubei, China, in 1989. She received the M.S. degree in optical engineering from the Wuhan Institute of Technology, Wuhan, China, in 2015, and the Ph.D. degree in optical engineering from Shenzhen University, Shenzhen, China, in 2018. From 2018 to 2020, she was with Information and Communication Engineering, Shenzhen University, as a Postdoc Research Fellow. Since September 2020, she has been with Shenzhen University, as an Assistant Professor. She has authored or coauthored have more than 30 journal and conference papers. Her research focuses on distributed optical fiber sensing technology.

Pengfei Li was born in Henan, China, in 1991. She received the M.S. degree from the School of Physics and Engineering, Henan University of Science and Technology, Luoyang, China, in 2019. She is currently working toward the Ph.D. degree in optical engineering with Shenzhen University, Shenzhen, China.

Yanjie Meng was born in Guang ling, China, in 1994. He received the B.Eng. degree in geomatics engineering from Southeast University, Nanjing, China, in 2016, and the M.S. degree from the China University of Mining and Technology, Xuzhou, China, in 2019. He is currently working toward the Ph.D. degree in optical engineering with Shenzhen University, Shenzhen, China. His main research interests include distributed optical fiber sensing and femtosecond laser processing.

Huajian Zhong was born in Jiangxi, China, in 1998. He received the B.S. degree from the Changchun University of Science and Technology, Changchun, China, in 2020. His research focuses on distributed optical sensing.

Bin Du was born in Henan, China, in 1992. He received the B.S. degree in flight vehicle propulsion engineering from the School of Astronautics, Bei hang University, Beijing, China, in 2016. His research interests include fiber vibration and ultrasound sensor.

Kuikui Guo was born in Henan, China, in 1988. He received the B.S. degree from the Institute of Photoelectric Information, Changchun University of Science and Technology, Changchun, China, in 2013, and the Ph.D. degree in optical engineering from Shenzhen University, Shenzhen, China, in 2020. From 2013 to 2015, he was an Optical Engineer with Accu-Tech Co. Ltd, Beijing, China. Since 2020, he has been a Postdoctoral Researcher with the Guangdong and Hong Kong Joint Research Centre for Optical Fiber Sensors, Shenzhen University. His research interests include optical fiber laser sensors and fiber Bragg gratings.

Lin Chen was born in Guangxi, China, in 1998. He received the B.S. degree from the Nanyang Institute of Technology, Singapore, in 2020. His research interests include fiber gratings and femtosecond laser processing.

Yiping Wang (Senior Member, IEEE) was born in Chongqing, China, in 1971. He received the B.Eng. degree in precision instrument engineering from the Xi'an Institute of Technology, Xi'an, China, in 1995, and the M.S. and Ph.D. degrees in optical engineering from Chongqing University, Chongqing, China, in 2000 and 2003, respectively. From 2003 to 2005, he was a Postdoctoral Fellow with Shanghai Jiao Tong University, Shanghai, China. From 2005 to 2007, he was a Postdoctoral Fellow with Hong Kong Polytechnic University, Hong Kong. From 2007 to 2009, he was a Humboldt Research Fellow with the Institute of Photonic Technology, Jena, Germany. From 2009 to 2011, he was a Marie Curie Fellow with the Optoelectronics Research Centre, University of Southampton, Southampton, U.K. Since 2012, he has been with Shenzhen University, Shenzhen, China, as a Distinguished Professor. He has authored or coauthored one book, 21 patent applications, and more than 240 journal and conference papers. His research interests include optical fiber sensors, fiber gratings, and photonic crystal fibers. Prof. Wang is a Senior Member of the Optical Society of America and Chinese Optical Society.

Jun He (Member, IEEE) was born in Hubei, China, in 1985. He received the B.Eng. degree in electronic science and technology from Wuhan University, Wuhan, China, in 2006, and the Ph.D. degree in electrical engineering from the Institute of Semiconductors, Chinese Academy of Sciences, Beijing, China, in 2011. From 2011 to 2013, he was a Research Engineer with Huawei Technologies, Shenzhen, China. From 2013 to 2015, he was affiliated with Shenzhen University, Shenzhen, China, as a Postdoctoral Research Fellow. From 2015 to 2016, he was a Visiting Fellow with The University of New South Wales, Sydney, NSW, Australia. Since 2017, he has been an Assistant Professor with Shenzhen University. He has authored or coauthored four patent applications and more than 80 journal and conference papers. His research interests include optical fiber sensors fiber Bragg gratings, and fiber lasers. He is a Member of the Optical Society of America.